PTRAN, a Monte Carlo code for transport simulation of 50 to 250 MeV protons
&
PTRAN_MEDIA, PTRAN_CAVITY and PTRAN_RZ, a series of derived codes

Hugo Palmans

National Physical Laboratory, Queens Road, Teddington, Middlesex TW11 0LW, UK

1. Abstract

PTRAN is a class I Monte Carlo code for proton transport in the energy range of clinical proton beams. Its application is restricted to the simulation of pencil beams in homogeneous water and the calculation of depth dose data, radial dose and fluence deposition data and spectral distributions as a function of depth.
We started using this code with the purpose of calculating perturbation factors of various detectors in proton beams in a time that MCNP didn't provide proton transport and GEANT had not developed its low-energy transport modules. To this end, various modifications were applied in the course of many years resulting in a number of codes that essentially use PTRAN's step, multiple scattering and energy loss sampling algorithms, but in which the geometry testing algorithms and scoring procedures were developed independently from the original program. The modifications allow the simulation of transport in other materials than water, broad beams with various geometrical and energy distributions, through cavities, in rz-voxel geometries and also allowed dynamic geometries such as a range modulator wheel.
In the first part of the presentation, the possibilities and principles of the original PTRAN code will be explained. In the second part, the implementation of the various adaptations, which resulted in the codes PTRAN_MEDIA, PTRAN_CAVITY and PTRAN_RZ, will be described and their use to dosimetry will be illustrated.
We are aware that the PTRAN code might be of rather limited general use, but we would like to present this as an illustration of how with some effort in understanding the basic concepts and principle algorithm of the code it is fairly easy to adapt it in order to use it in a flexible way for one's own purposes.

2. PTRAN – calculation of ppds in water

PTRAN [1] uses the Monte Carlo method to simulate the transport of proton beams through water. Details on the use of the programs and the methods used in the Monte Carlo transport are given by Berger [1]. A brief summary is given in this section.
The incident proton energies for which the code is designed range from 50 to 250 MeV, although it is applicable to a wider range of energies. PTRAN contains several cross section preparation programs and two main codes, PTRAN3D and PTRAN1D. The code take into account multiple scattering and Coulomb interaction energy loss mechanisms along with non-elastic nuclear interactions. Deposition of energy as a function of depth and radial distance from the beam as well as energy spectra of the primary protons as function of depth are scored.

The simulations follow a class I condensed random walk scheme [2] in which each proton is transported down to a cut-off energy by dividing its track in a series of short steps. They are based on a precalculated energy grid at which the various cross section and probability distributions are evaluated. The following distributions are used:

(i) Energy losses in Coulomb collisions with atomic electrons are sampled from the Vavilov energy straggling distribution [3] using the ICRU report 49 stopping powers [4] as average values.
(ii) Multiple scattering deflections due to elastic scattering by atoms are sampled from the Molière distribution [5].
(iii) Energy losses in non-elastic nuclear interactions are based on fits to experimental data [6, 7] based on theoretical considerations [8].

2.1. Cross-section preparation programs

2.1.1. PARAM calculates grids and various parameters:

(i) An energy grid with energy steps $\Delta T_i = T_i - T_{i+1}$ which are either a constant value ΔT or $k \cdot T_i$ (whichever is smaller) down to a chosen cut-off energy T_{cut}.
(ii) The path length for each energy interval in the continuous slowing down approximation (CSDA) using ICRU 49 stopping powers.
(iii) Parameters for calculating the Vavilov distribution at T_i.
(iv) Parameters for calculating the Molière distribution at $(T_i + T_{i+1})/2$.
(v) Nuclear absorption coefficients, representing the probability per unit path length of a non-elastic nuclear interaction, are calculated from the non-elastic nuclear cross sections. From these, CSDA survival weight factors are derived as a function of energy T_i, which thus represent the fraction of protons (on the average) that has not undergone a non-elastic nuclear interaction when slowed down from energy T_0 to T_i.

2.1.2. VPREP calculates the Vavilov distribution for each grid energy T_i. The data are prepared for enabling sampling using the alias sampling method.

2.1.3. MPREP calculates the Molière distribution for each grid energy T_i [at $(T_i + T_{i+1})/2$]. The data are prepared for enabling sampling using the alias sampling method.

2.2. Transport algorithm of PTRAN3D

The following scheme is applied:

(i) All protons start at $(x,y,z) = (0,0,0)$ in the direction of the z-axis (polar axis) with an energy E_1 which can be specified at the start of the program.
(ii) In the n^{th} step, the proton starts with and energy E_n and a direction characterised by a polar angle θ_n and an azimuthal angle φ_n, both with respect to the initial direction of the protons at the 1^{st} step (laboratory coordinate system).
(iii) The energy loss $E_n - E_{n+1}$ is sampled from the Vavilov distribution at the energy grid value T_i that is nearest to E_n.
(iv) The path length Δs_n is calculated by interpolating to the energy E_n in the path length versus T_i table.

(v) The multiple-scattering angular deflection is sampled by sampling and angle θ' from the Molière distribution for the energy grid interval $[T_i,T_{i+1}]$ and φ' from a uniform distribution between –180 and +180 degrees. θ' and φ' are both specified in a coordinate system $x'y'z'$ whose polar axis coincides with the direction of the proton at the beginning of the step and are converted to angles θ_n and φ_n at the end of the step by a rotational transformation.

(vi) The displacements in the coordinate system $x'y'z'$ are calculated and transformed into displacements Δx, Δy and Δz in the laboratory coordinate system by the same rotational transformation.

(vii) If the energy E_{n+1} is lower than the cut-off energy E_{cut} or a final energy E_{fin}, defined upon starting the calculation, the remaining energy of the particle is binned in a track-end array.

2.3. Scoring geometry – scoring method

A set of scoring planes is defined perpendicular to the direction of the incident proton beam as shown in figure 1. The depths z_i of these planes are defined in terms of the CSDA range r_0. In each plane, an array of concentric radial bins with centre $(x,y) = (0,0)$ is defined for the scoring of radial energy deposition distributions as well as an array of energy bins for the scoring of spectra. The positions of the scoring planes and the radial and energy bins are defined in a boundary input file.

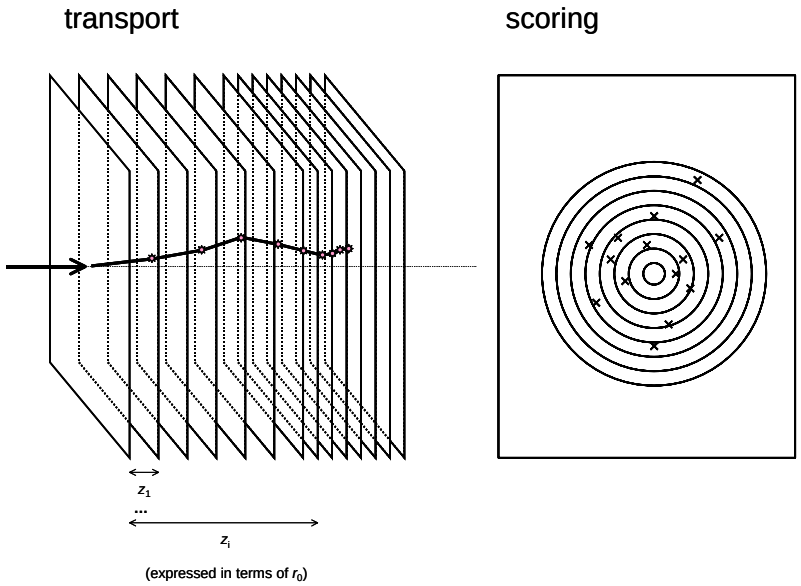

Figure 1. Scoring geometry of PTRAN3D.

If a step during the transport simulation of a proton traverses one of the defined scoring planes, the energy E_{cross}, the lateral position (x_{cross},y_{cross}) and the polar angle θ_{cross} are determined by linear interpolation between the conditions at the beginning and at the end of the step. The survival factor W_{cross}, the stopping power S_{cross} and the nuclear absorption factor μ_{cross} are then evaluated at the energy E_{cross}. The following quantities are then scored:

(i) the energy loss in Coulomb interactions, $(dE/dz)_C$, estimated as $S_{cross} \cdot W_{cross}/\cos\theta_{cross}$,

(ii) the energy loss in non-elastic nuclear interactions, $(dE/dz)_N$, estimated as $E_{cross} \cdot \mu_{cross} \cdot W_{cross} / \cos\theta_{cross}$,

(iii) the fluence estimated as $1/\cos\theta_{cross}$.

The fluence is binned in the energy spectra and $(dE/dz)_C$ in the radial bins. Since the energy transferred in non-elastic nuclear interactions is only partially going to charged particles (the rest is escaping through neutrons and photons) this fraction can be taken into account in a post-processing program PTSUM. In this, the energy transferred to secondary charged particles is deposited at the position where they are generated. This is a crude approximation, which is not accurate for high-energy protons where secondary proton disequilibrium has a significant effect on dose distributions.

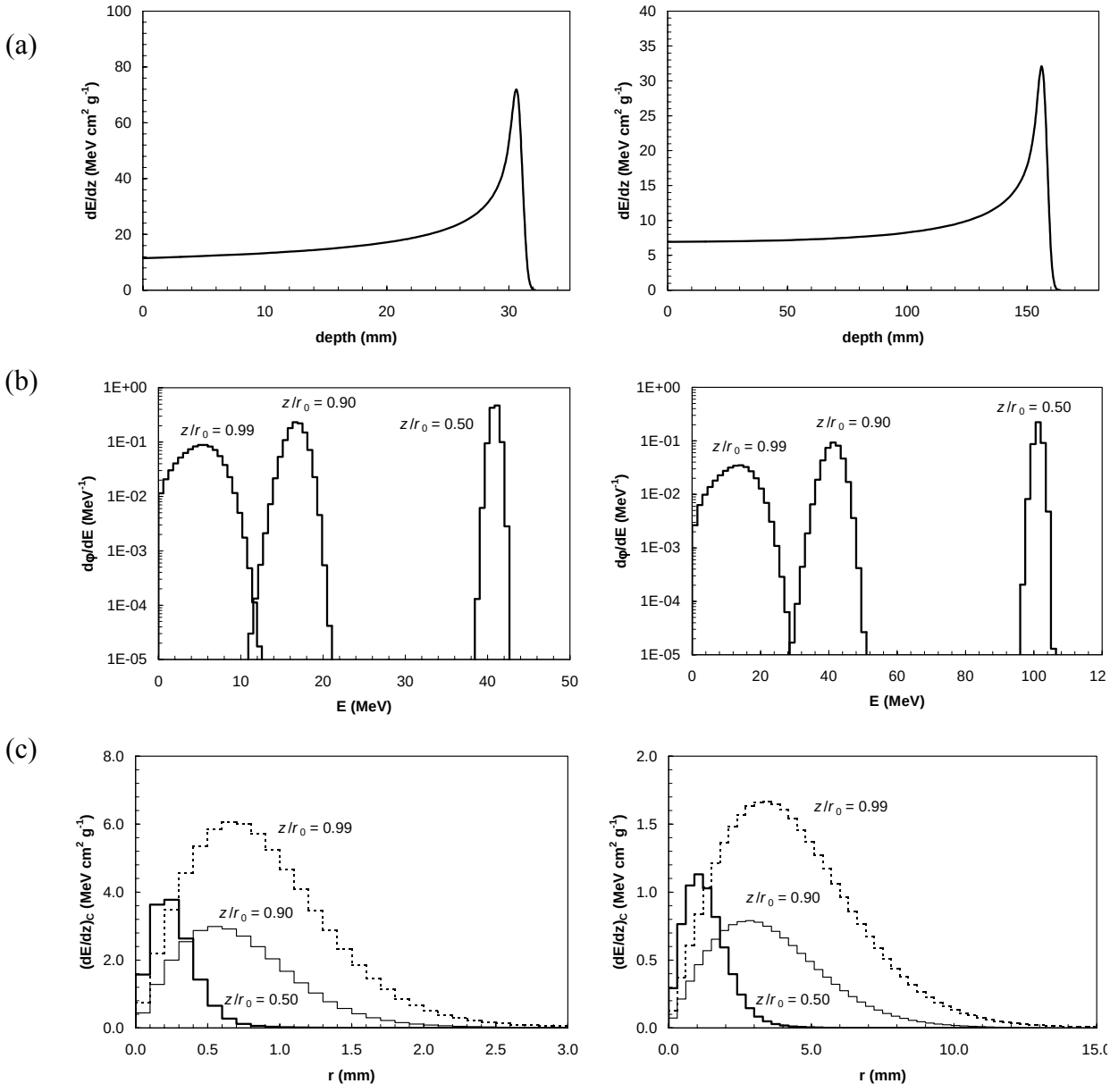

Figure 2 (a) calculated depth dose data with PTRAN3D, (b) spectral fluence distributions and (c) radial energy deposition data for a 60 MeV beam (left) and a 150 MeV beam (right).

2.4. Random numbers

Two random number generators are foreseen with PTRAN:

(i) A congruential generator which requires only two statements:

IR=IAND(MASK,IR*MULT)
R=RNORM*IR

where RNORM = 2^{-31} = 4.656612873E-10 and MASK = 2147483647
PTRAN3D uses two random number sequences with different MULT values the period of the sequence is about 5.37E+08

(ii) The lagged Fibonacci random number generator

2.5. Example calculation

Figure 2 shows depth distributions of $(dE/dz)_C$ and $(dE/dz)_N$, spectral fluence distributions and radial energy deposition distributions at a few depths for incident proton energies of 60 MeV and 150 MeV beam.

3. PTRAN_MEDIA – calculation of pdds in other materials, inhomogeneous slab geometries and for modulated beams

PTRAN_MEDIA is a modified version of PTRAN3D, which allows the simulation of

(i) other materials than water
(ii) inhomogeneous slab geometries
(iii) broad and non mono-energetic beams
(iv) the dynamic feature of a modulator wheel.

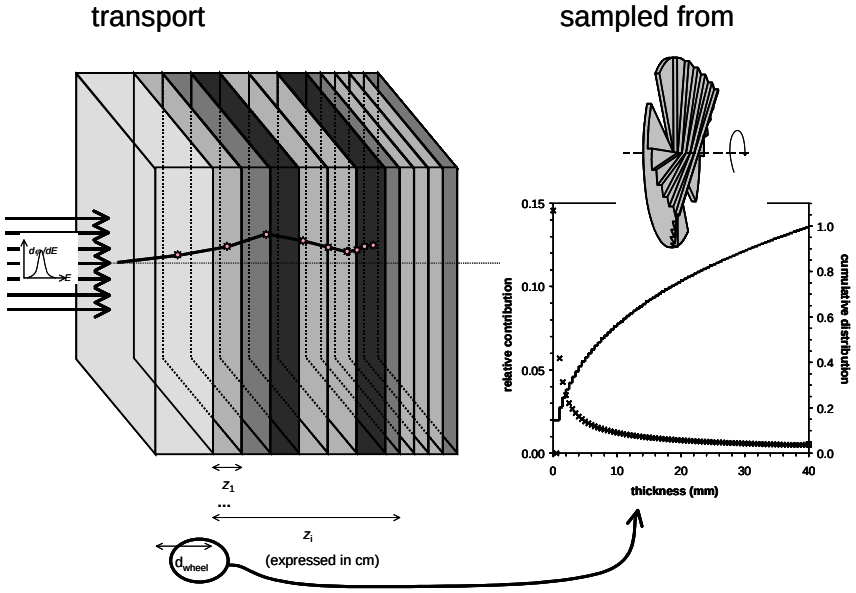

Figure 3 Scoring geometry of PTRAN_MEDIA.

This code was developed in three stages for different applications over time. The geometry for this code is shown in figure 3 and will be explained in the next subsections, following the three-stage chronology of the development.

3.1. Other materials than water

3.1.1. Implementation This is mainly a matter of including the data for those materials.

(i) For most materials of interest, stopping powers can be taken directly from ICRU report 49 [4]. For materials not listed in there, Bragg's additivity rule can be applied although a recent paper [9] shows that some refinements are required in order to be consistent concerning the calculation of the mean excitation energy I_0 and the Barkas correction.

(ii) The calculation of the Vavilov distribution require the first moments S_1 and I_1 of the oscillator strength distribution and the mean excitation energies for the calculation of a small correction to the theory introduced by Shulek [10]. S_1 and I_1 were taken from Inokuti et al [11, 12] for all elements with Z ranging from 1 to 38. Bragg's rule was applied for compounds.

(iii) For the calculation of the Molière multiple scattering distributions, a correction factor k_{HF} has to be applied to the screening angle. These data were taken from Berger and Wang [13].

(iv) Non-elastic nuclear interaction cross sections were taken from Janni [14] and ICRU report 63 [15] in the studies described below. For the elements not specified in these references, log-log interpolation of the cross sections as a function of the atomic number was used. In recent work, only the ICRU report 63 data have been considered since they form a more comprehensive set. Apart from gathering the required data, some technical modifications to the coding of the cross section preparation programs.

(v) In addition, the range of incident beam types was extended from only mono-directional and mono-energetic beams to circular beams, rectangular beams, beams with an angular distribution and beams with a Gaussian energy distribution.

3.1.2. Application: fluence correction factors IAEA TRS-398 [16] recommends to perform reference dosimetry with ionisation chambers in a water phantom. However, when performing dosimetry in low-energy beams, it could be necessary to do the measurements in a plastic phantom in order to achieve sufficiently accurate positioning. A fluence correction factor should then be introduced to account for any difference in fluence at equivalent depths in the plastic phantom and in water. This situation can be compared with the one for electron beams. A preparatory study showed that differences in scaled depth dose curves between different materials were almost entirely due to differences in non-elastic nuclear interaction cross sections [17]. PTRAN_MEDIA was used to evaluate fluence correction factors for PMMA and polystyrene and compare these values with experimental results [18]. Later, fluence correction factors were calculated for graphite to examine the water equivalence of graphite in calorimetry [19,20], for alanine [21] regarding the measurement of depth dose curves with alanine pellets and for some ICRU tissue specifications to evaluate the importance of incorporating material dependent non-elastic nuclear interaction data in treatment planning [22]. Results are shown in figure 4.

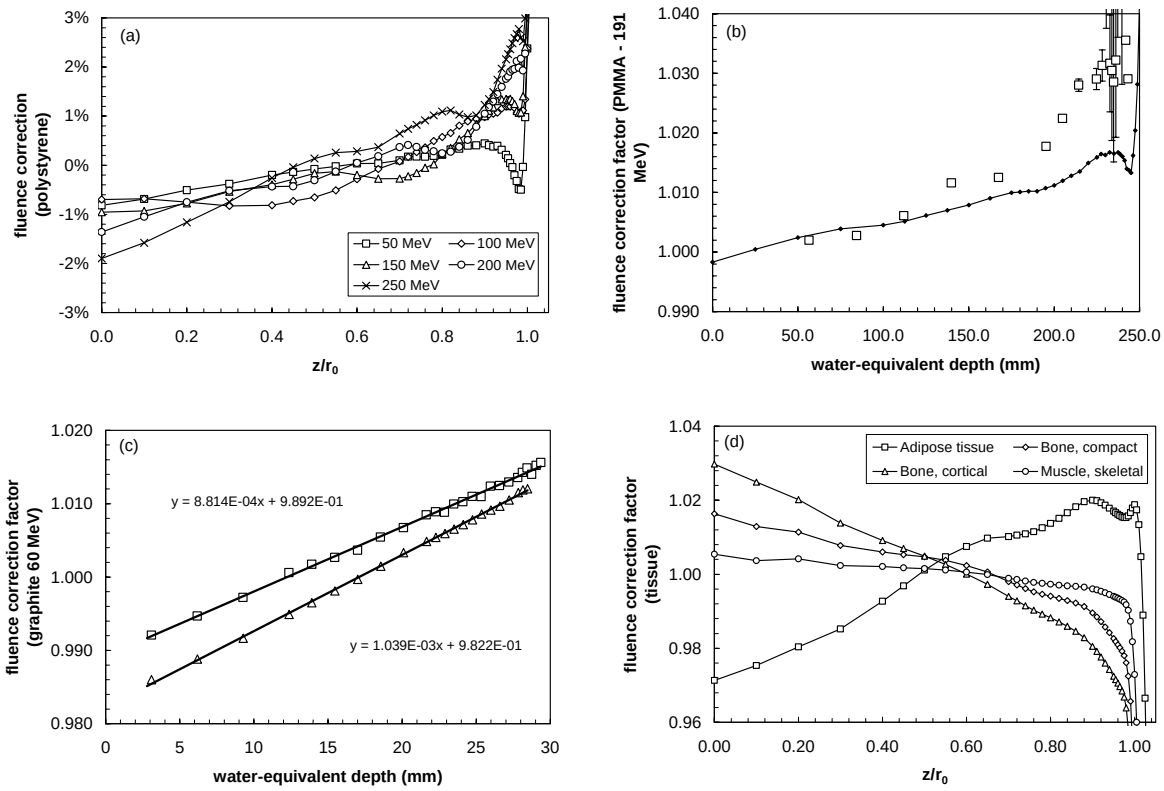

Figure 4. Fluence perturbation correction factors for (a) polystyrene in various energies (adapted from [18]), (b) PMMA in a 191 proton beam (squares: experimental results - adapted from [18]), (c) graphite in 60 MeV (non-modulated and modulated - adapted from [20]), (d) some ICRU defined tissues in 250 MeV.

3.2. Boundary crossing algorithm

3.2.1. Implementation The technical changes required for this implementation are:

(i) When a boundary is encountered in a particle's trajectory, the particle is transported to the boundary along the trajectory. The energy loss along the track is scaled with the ratio of the step length up to the boundary to the initially sampled step length. At the boundary, the energy E_{bound}, the polar angle θ_{bound} and the survival factor W_{bound}, are evaluated in the same way as the scoring plane crossing quantities (section 2.3). Given the small scattering angles and energy losses that are involved, we can assume that the errors due to this approximation are small. An evaluation of the influence of the step-cutting artefact revealed no significant effect [23]. For the next step, new multiple scattering angles and energy loss are calculated based on the material properties of the new region.

(ii) The expression of all distances in cm instead of scaled with r_0.

(iii) Giving all material dependent data an additional array dimension.

(iv) Administration of the media information for each layer defined by two scoring planes.

3.2.2. Application: dose in an inhomogeneity An example will be given; the dose in a bone slab from a calculation in homogeneous water versus from a calculation in the inhomogeneous situation is compared [22].

3.3. Dynamic geometries – modulator wheels

3.3.1. Implementation As illustrated in figure 3, the implementation of a modulator wheel is done by including an additional layer at the front of the geometry. For each incident proton, the thickness of this layer is sampled from the distribution of the wheel thickness. The incident proton is then set in motion at the front of this additional layer. The usual situation where the wheel is a long distance away from the phantom can be easily dealt with by defining the second layer as air with the thickness equalling the distance between the modulator wheel and phantom.

3.3.2. Application: spectra and stopping powers in modulated beams This feature of PTRAN_MEDIA was used to calculate spectral distributions for the calculation of the effective response of a TLD detector in a modulated beam [24] and for the calculation of proton stopping powers in a modulated beam [23]. The latter study showed that water to air stopping power ratios in a modulated beam down to distances of about 1.5 cm from the distal edge of the pdd were not more than 0.3% higher than in non-modulated mono-energetic proton beam at the same residual range R_{res} (the distance from the depth of the distal 10% dose level). This result was used in IAEA TRS-398 [16] to justify the use of a unique beam quality specifier and data set, common to both modulated and non-modulated proton beams. Example spectra in a modulated beam at various depths are shown in figure 5.

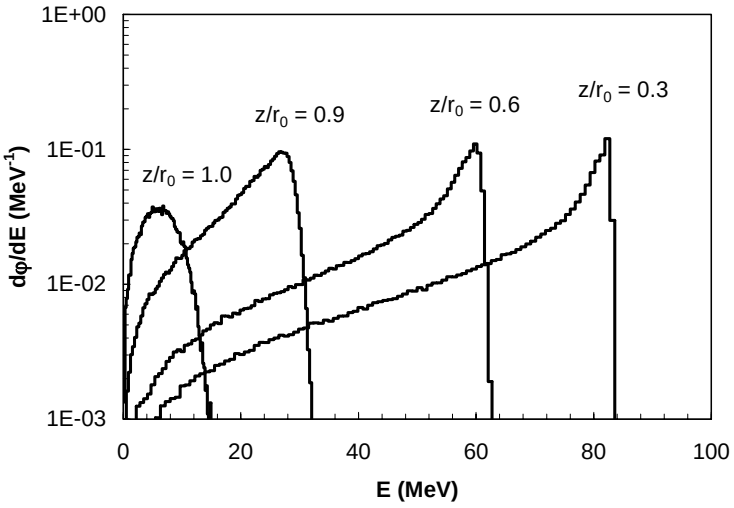

Figure 5. Spectral fluence distributions in a 100 MeV modulated proton beam at various depths in water normalised per incident proton (adapted from [23]).

4. PTRAN_CAVITY – calculation of doses in cavities

4.1. Further changes

The existing scoring algorithm in PTRAN3D is inconvenient for calculating doses in inhomogeneous geometries that are more complex than slab geometries. In the next stage, the original scoring algorithm was abandoned and cylindrical and spherical cavity geometries were introduced, with the specific purpose of simulating ionisation chamber perturbations, hence, this version of the code has been called PTRAN_CAVITY. Essentially, all elements from the existing geometry in PTRAN_MEDIA were retained. Although the scoring planes have no function in the scoring algorithm any more, they proved to be useful for geometry interrogation reduction. In between two of the existing scoring planes a number of non-intersecting and embedded spherical and/or cylindrical cavities can be defined. The situation of two concentric cylindrical cavities is illustrated in figure 6.

4.1.1. Scoring algorithm The following scoring features are implemented:

(i) In each geometrical region, the track length can be scored and binned into an energy spectrum. The boundary-crossing algorithm assumes that track length is distributed evenly along the step.
(ii) The energy loss is calculated as the difference between the begin and end energy of the step (whether it be a 'normal' or a cut-off step).
(iii) The non-elastic nuclear energy transfer is scored at the average value of the energies at begin and end of the step.
(iv) If desired, both quantities in the previous two steps can be binned as a function of energy as well.

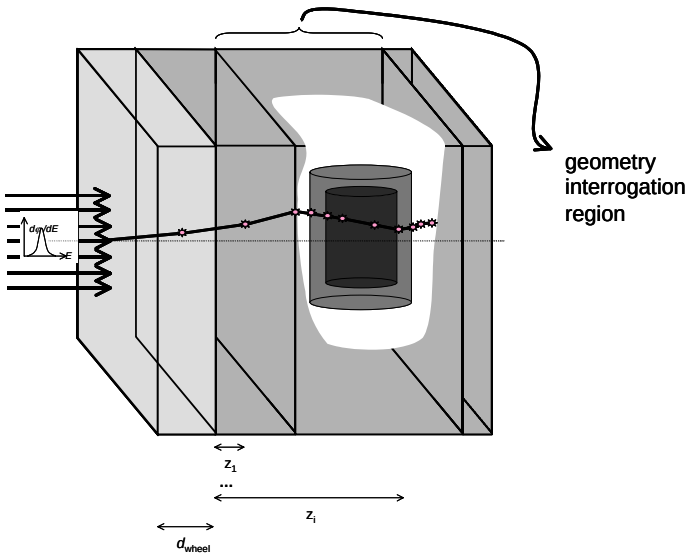

Figure 6. Geometry with dynamic modulator wheel and two concentric cylindrical cavities.

4.2.2. Geometry interrogation and correlated sampling A geometry interrogation reduction method is used to avoid unnecessary testing. The test whether or not a particle enters a cavity is only activated in a region between two slabs where the cavities have been specified. This results in a substantial reduction of calculation time.

A correlated-sampling technique was implemented as well, to allow a more efficient calculation of perturbation factors for ionisation chambers with equal geometries but different wall materials. Practically this means that when a particle enters the cavity that defines the outer dimensions of the ionisation chamber wall, the energy, the spatial coordinates and directional coordinates of the proton are stored as well as the random numbers of the simulation at that point. After the transport of that particle is finished, the transport simulation is restarted with the stored conditions but with the wall set to another material. This approach not only saves computing time but also improves the statistical correlation of the doses in the cavity with and without wall (in which case the wall material is set to the surrounding medium).

4.2. Applications

4.2.1. Gradient correction factors for ionisation chambers The response of a graphite walled NE2571 ionization chamber was measured as a function of wall thickness in a PMMA phantom. To this end, four graphite build-up caps (serving as sleeves to increase the apparent wall thickness) and corresponding PMMA holders to fit in the phantom were constructed. The thicknesses of the build-up caps were 1.5 mm, 2.5 mm, 4.5mm and 9.5 mm. The measured dose response as a function of wall thickness was compared with Monte Carlo calculated values using PTRAN_CAVITY. The results, reported in [25], are shown in figure 7. This code was used to calculate the effective point of measurement for a number of ionisation chamber types [26,27]

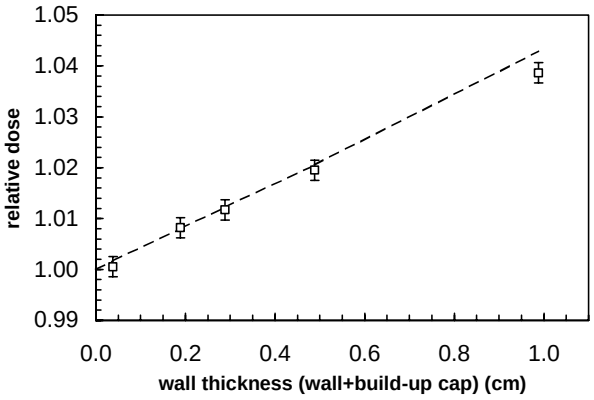

Figure 7. Monte Carlo calculated (dashed line) and measured (symbols) variation of the ionisation chamber signal as a function of graphite wall thickness (reproduced from [25]).

4.2.2. Secondary electrons perturbation correction factors for ionisation chambers The track lengths scored in a volume can be used to evaluate the probability distribution of the generation of δ-electrons with energies above a certain threshold (1 keV in this case). This method was used to calculate the amount of energy that was transported out of the air cavity of an ionisation chamber by electrons and the amount of energy that was imported from the surrounding regions (wall, sleeve and medium) [28]. The Bahba cross-section for the generation of secondary electrons was used [29] and the transport of these electrons was simulated with EGSnrc [30]. That way, δ-electron perturbation correction factors were calculated for ionisation chambers and the results were compared with experimental data [25] shown in figure 8.

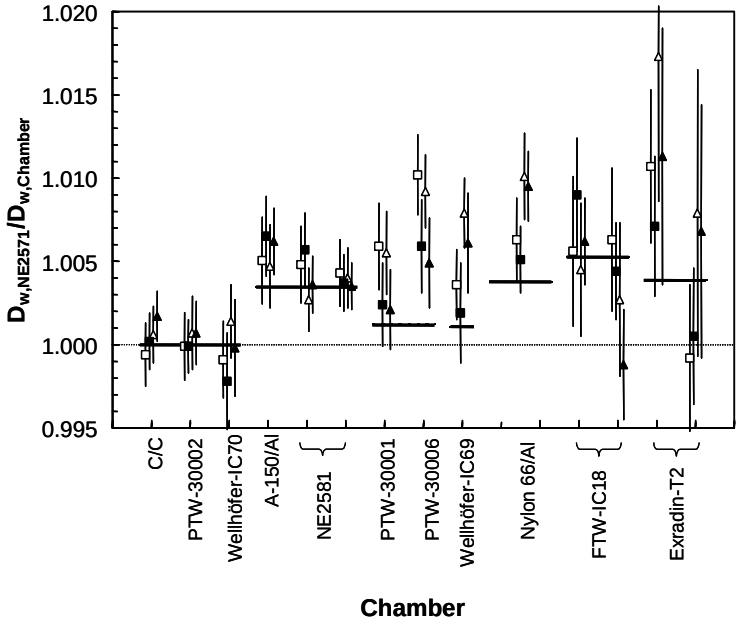

Figure 8. Comparison of the $p_{wall,e}$-ratios (relative to the NE2571 chamber) calculated using Monte Carlo (thick horizontal lines) and obtained experimentally in a 75 MeV proton beam. Square symbols are for a non-modulated beam, triangles for a modulated beam, open symbols are based on absorbed dose calibrations and full symbols based on air kerma calibrations (Adapted from [31]).

5. PTRAN_RZ – calculation of doses in rz-geometry

5.1. Geometry

With all the information in the previous sections, the implementation of an rz-voxel geometry is straightforward. The slab geometry is retained and a number of concentric cylinders are constructed perpendicularly to the slabs. In each of the rz-voxels, a different medium can be specified and the same quantities as in PTRAN_CAVITY can be scored. The geometry is shown in figure 9.

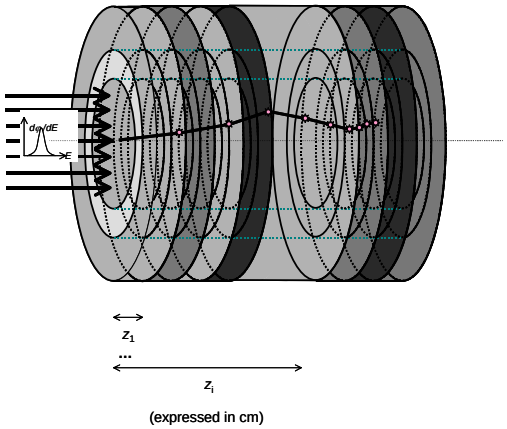

Figure 9. Geometry used in PTRAN_RZ.

5.2. Application: pdds measured with alanine pellets

Figure 10 shows the application to a stack of alanine pellets in a PMMA phantom. This simulation was performed to investigate the source of the tail beyond the Bragg peak. The agreement is fine up to the beginning of the Bragg peak. In the Bragg peak there seems to be an under response of the alanine dosimeters which is consistent with other results in the literature [9]. The tail in the calculation is the result of in scatter from the surrounding medium and under predicts the effect. The remainder of the measured signal might be due to tunnelling of protons through the air gap between the pellets and the PMMA phantom [9,32].

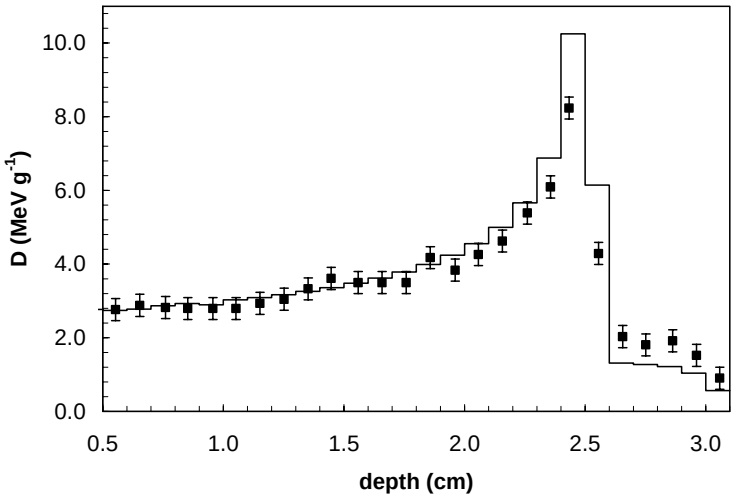

Figure 10. Dose in a stack of alanine pellets in a PMMA phantom, measured (symbols) [32] and calculated with PTRAN_RZ using a Gaussian energy distribution with a mean value of 62 MeV and a variance of 0.5% (line).

References

[1] Berger, M. J. (1993) "Proton Monte Carlo transport program PTRAN." *National Institute for Standards and Technology Report* NISTIR 5113 (Gaithersburg, USA: NIST)

[2] Berger, M. J. (1963) "Monte Carlo calculation of the penetration and diffusion of charged particles" in *Methods in computational physics*, Vol. 1, Ed. Alder, B., Fernbach, S. and Rotenberg, M., pp. 135-215 (New York, USA: Academic Press).

[3] Vavilov, P. V. (1957) "Ionization losses of high-energy particles." *Sov. Phys.-JETP* 5:749-751

[4] ICRU (1993) "Stopping powers and ranges for protons and alpha particles." *International Commission on Radiation Units and Measurements Report 49* (Bethesda, USA: ICRU)

[5] Molière, G. Z. (1948) "Theorie der Streuung schneller geladener Teilchen. II. Mehrfach- und Vielfachstreuung." *Z. Naturforsch* 3a:78 – 97

[6] Renberg, P. U., Measday, D. F., Pepin, M., Schwaller, P., Favier, B. and Richard-Serre, C. (1972) "Reaction cross sections for protons in the energy range 220-570 MeV." *Nucl. Phys. A* 183:81-104

[7] Carlson, R. F., Cox, A. J., Nimmo, J. R., Davison, N. E., Elbakr, S. A., Horton, J. L., Houdayer, A., Sourkes, A. M., Van Oers, W. T. H. and Margaziotis, D. J. (1975) "Proton

total reaction cross sections for the doubly magic nuclei O-16, Ca-40 and Pb-208 in the energy range 20-50 MeV." *Phys. Rev. C* 12:1167-1175

[8] Seltzer, S. M. (1993) "An assessment of the role of charged secondaries from nonelastic nuclear interactions by therapy proton beams in water." *National Institute for Standards and Technology Report* NISTIR 5221 (Gaithersburg, USA: NIST)

[9] Palmans, H. (2003) "Effect of alanine energy response and phantom material on depth dose measurements in ocular proton beams." *Technol. Cancer Res. Treat.* 2:579-586

[10] Shulek, P., Golovin, B. M., Kolyukina, L. A., Medvedev, S. N. and Pavlovich, P. (1966) "Fluctuation of ionization losses." *J. of Nucl. Phys.* 4:564-566 (in Russian)

[11] Inokuti, M., Baer, T. and Dehmer, J. L. (1978) "Systematics of moments of dipole oscillator-strength distributions for atoms in the first and second row." *Phys. Rev. A* 17:1229-1231

[12] Inokuti, M., Dehmer, J. L., Baer, T. and Hanson, J. D. (1981) "Oscillator-strength moments, stopping powers and total inelastic-scattering cross sections of all atoms through strontium." *Phys. Rev. A* 23: 95-109

[13] Berger, M. J. and Wang, R. (1988) "Multiple-scattering angular deflections and energy-loss straggling." in *Monte Carlo Transport of Electrons and Photons* Ed. Jenkins, T. M., Nelson and W. R., Rindi, p. 21 – 56 (New York, USA:Plenum Press)

[14] Janni, J. F. (1982) "Proton range-energy tables, 1 keV - 10 GeV." *Atom. Data Nucl.Data Tables* 27:147-339

[15] ICRU (2000) "Nuclear data for neutron and proton radiotherapy and for radiation protection dose." *International Commission on Radiation Units and Measurements Report 63* (Bethesda, USA: ICRU)

[17] Palmans, H. and F. Verhaegen (1997), "Calculated depth dose distributions for proton beams in some low-Z materials." *Phys. Med. Biol.* 42:1175-1183

[18] Palmans, H., J. E. Symons, J-M. Denis, E. A. de Kock, D. T. L. Jones and S. Vynckier (2002) "Fluence correction factors in plastic phantoms for clinical proton beams." *Phys. Med. Biol.* 47:3055-3071

[19] Palmans, H., Thomas, R., Simon, M., Duane, S., Kacperek, A., Seco, J., Nutbrown, R., Shipley, D., DuSautoy, A. and Verhaegen, F. (2004) "Feasibility of graphite calorimetry in a modulated low-energy clinical proton beam." *Proceedings of the Workshop on Recent Advances in Absorbed Dose Standards* held at ARPANSA, Melbourne, Australia, 19-21 August 2003

[20] Palmans, H., Thomas, R., Simon, M., Duane, S., Kacperek, A., DuSautoy, A. and Verhaegen, F. (2004) "A small-body portable graphite calorimeter for dosimetry in low-energy clinical proton beams." submitted to *Phys. Med. Biol.* (special issue on the World Conference on Medical Physics and Biomedical Engineering held in Sydney, Australia, 24-29 August 2003)

[21] Palmans, H. (2004) "Alanine dosimetry for ocular clinical proton beams." *NPL Internal report in preparation*

[22] Palmans, H., Shipley, D., Nutbrown, R. and Verhaegen, F. (2004) "Inelastic nuclear interactions in Monte Carlo simulations for clinical proton beams." *Abstracts of the 10th MCNEG meeting*, NPL, UK, 15-16 March 2004

[23] Palmans, H. and F. Verhaegen (1998), "Monte Carlo study of fluence perturbation effects on cavity dose response in clinical proton beams." *Phys. Med. Biol.* 43:65-89

[24] Palmans, H., Olko, P., Bilski, P. and Heese, J. (1997) "Calculations of relative dose deposition and primary proton spectra in LiF-TLD's in a 70 MeV proton beam." *Med. Biol. Eng. Comput.* 35(suppl. 2): 975

[25] Palmans, H., Verhaegen, F., Denis, J.-M., Vynckier, S. and Thierens, H. (2001) "Experimental pwall and pcel correction factors for ionization chambers in low-energy clinical proton beams." *Phys. Med. Biol.* 46:1187-1204

[26] Palmans, H. and Verhaegen, F. (2000) "On the effective point of measurement of cylindrical ionization chambers for proton beams and other heavy charged particle beams." *Phys. Med. Biol.* 45:L20-L22

[27] Palmans, H. (2000) "Analytical expressions for the determination of the effective water depth of an ionization chamber for clinical proton beam dosimetry." *CD-ROM Proceedings of the World Congress on Medical Physics and Biomedical Engineering* Chicago, USA, July 23-28 2000, 4 pp

[28] Verhaegen, F. and Palmans, H. (2001) "A systematic Monte Carlo study of secondary electron fluence perturbation in clinical proton beams (70-250 MeV) for cylindrical and spherical ion chambers." *Med. Phys.* 28:2088-2095

[29] Bahba, H. J. (1938) "On the penetrating component of cosmic radiation." *Proc. Roy. Soc.* A164:257-294

[30] Kawrakow, I. (2000) "Accurate condensed history Monte Carlo simulation of electron transport. I. EGSnrc, the new EGS4 version." *Med. Phys.* 27:485-498

[31] Palmans, H. and Verhaegen, F. (2002) "Calculation of perturbation correction factors for ionization chambers in clinical proton beams using proton-electron Monte Carlo simulations and analytical model calculations," in *Recent developments in accurate radiation dosimetry* Ed. Seuntjens, J. P. and Mobit, P. N., pp. 229-245 (Madison WI, USA: Medical Physics Publishing)

[32] Onori, S., d'Errico, F., De-Angelis, C., Egger, E., Fattibene, P. and Janovsky, I. (1997) "Alanine dosimetry of proton therapy beams." *Med. Phys.* 24:447-453